General Disclaimer

One or more of the Following Statements may affect this Document

- This document has been reproduced from the best copy furnished by the organizational source. It is being released in the interest of making available as much information as possible.

- This document may contain data, which exceeds the sheet parameters. It was furnished in this condition by the organizational source and is the best copy available.

- This document may contain tone-on-tone or color graphs, charts and/or pictures, which have been reproduced in black and white.

- This document is paginated as submitted by the original source.

- Portions of this document are not fully legible due to the historical nature of some of the material. However, it is the best reproduction available from the original submission.

Produced by the NASA Center for Aerospace Information (CASI)

$Tmx-71368$

A FOURIER APPROACH TO CLOUD MOTION ESTIMATION

ALBERT ARKING
ROBERT C. LO
AZRIEL ROSENFELD

JUNE 1977

GSFC —— **GODDARD SPACE FLIGHT CENTER** ——
GREENBELT, MARYLAND

A FOURIER APPROACH TO CLOUD MOTION ESTIMATION

Albert Arking

Goddard Space Flight Center

Greenbelt, Md. 20770

Robert C. Lo* and Azriel Rosenfeld

Computer Science Center

University of Maryland

College Park, Md. 20742

June 1977

GODDARD SPACE FLIGHT CENTER

Greenbelt, Md. 20770

A FOURIER APPROACH TO CLOUD MOTION ESTIMATION

Albert Arking

Goddard Space Flight Center

Greenbelt, MD 20770

Robert C. Lo* and Azriel Rosenfeld

Computer Science Center

University of Maryland

College Park, MD 20742

ABSTRACT

A Fourier technique for cloud motion estimation from pairs of pictures is described. This technique makes use of the phase of the cross spectral density; it allows motion estimates to be made for individual spatial frequencies, which are related to cloud pattern dimensions. Results obtained using this technique are presented and are compared with the results of a Fourier-domain cross-correlation scheme, using both artificial and real cloud data. It is concluded that this technique is relatively sensitive to the presence of mixtures of motions, changes in cloud shape, and edge effects.

*Present address: Computer Sciences Corp., Silver Spring, MD.

CONTENTS

ILLUSTRATIONS

CONTENTS (Cont'd)

A FOURIER APPROACH TO CLOUD MOTION ESTIMATION

I. INTRODUCTION

Sequences of high resolution photographs from satellites in geosynchronous orbit have been utilized by many investigators to measure cloud motion and derive winds. The techniques for extracting such information range from a manual analysis of closed "movie loops" (Fujita et al., 1969; Hubert and Whitney, 1971) to completely automated methods in which the images and/or data are computer processed but selection of cloud targets is controlled manually from an interactive display console (Serebreny et al., 1969; Smith and Phillips, 1972).

The main advantage of manual and semi-automatic methods is in target selection, making it possible to incorporate a wide variety of criteria, not necessarily defined beforehand, for choosing cloud elements representative of atmospheric motion. These criteria are sometimes related to the size of the cloud element, the idea being that small elements move with the wind, while massive elements may disguise the actual motion of the atmosphere due to cloud formation and deformation processes.

Early studies by Leese and Epstein (1963) have shown that one can identify the predominant dimensions of cloud patterns by a spectral analysis of satellite photographs. Subsequently, Leese et al. (1971) used the Fourier transform as an efficient computational tool for obtaining the cross-correlation between successive cloud cover pictures, from which cloud displacements are derived.

The fact that displacement information appears separately for each spectral component in the Fourier transform of the cross-covariance function was pointed out by Weinstein (1972). The combined advantages of the Fourier transform — as an efficient computational tool for measuring displacement and as a means for extracting cloud pattern dimensional information — have motivated the present study of the Fourier transform properties of real and simulated sequences of satellite cloud cover pictures and their cross-correlations. Specifically, we describe an attempt to derive winds from cloud motion, while discriminating with respect to cloud size.

The mathematical aspects of the Fourier transform method are outlined in Section 2; the results of a simulation study are presented in Section 3; a preliminary experiment with real pictures is described in Section 4; and finally, the outlook is discussed and conclusions drawn in Section 5.

II. PROPERTIES OF THE FOURIER TRANSFORM

A function defined in the space domain, say $f(x,y)$, where x and y are coordinates in a two-dimensional Cartesian space, can be transformed into a function in the frequency domain by using the Fourier transform, F, as follows:

$$F[f(x,y)] \equiv \int\int_{-\infty}^{\infty} f(x,y)\, e^{-2\pi i(ux+vy)}\, dx\, dy \equiv F(u,v) \tag{1}$$

where $i = \sqrt{-1}$; u and v are frequency domain variables. Conversely, a function

in the frequency domain can be transformed into the space domain by using the inverse Fourier transform:

$$F^{-1}[F(u,v)] \equiv \int\int_{-\infty}^{\infty} F(u,v) \, e^{2\pi i(ux+vy)} \, du \, dv \equiv f(x,y) \tag{2}$$

For application to discrete data, the Fourier transform process is redefined as

$$F(u,v) = \frac{1}{MN} \sum_{x=0}^{M-1} \sum_{y=0}^{N-1} f(x,y) \, e^{-2\pi i \left(\frac{ux}{M} + \frac{vy}{N}\right)} \tag{3}$$

$$f(x,y) = \frac{1}{MN} \sum_{u=0}^{M-1} \sum_{y=0}^{N-1} F(u,v) \, e^{2\pi i \left(\frac{ux}{M} + \frac{vy}{N}\right)} \tag{4}$$

where M and N are the sample sizes in the x and y directions, respectively.

One indication of the relative displacement between successive pictures is by the location of the peak of the cross-covariance of the two images (Leese et al., 1971). Letting f(x,y) and g(x,y) represent the brightness distribution of the two images, the cross-covariance is defined as

$$C_{fg}(x,y) = \int\int_{-\infty}^{\infty} f(\xi,\eta) \, g(\xi-x,\eta-y) \, d\xi \, d\eta \tag{5}$$

The Fourier transform provides a fast way to calculate the cross-covariance

function. From equations (1) and (2), it follows that

$$C_{fg}(x,y) = F^{-1}[F^*(u,v) \cdot G(u,v)] \qquad (6)$$

where $F^*(u,v)$ is the complex conjugate of $F(u,v)$ while $G(u,v)$ is the Fourier transform of $g(x,y)$. The Fourier transform of C_{fg}, namely F^*G, is called the cross spectral density of f and g. The positions of the maxima of the cross-covariance function determine the relative displacement between the two pictures. The ratio of the computer times required for the Fourier transform method and the conventional method of calculating the cross-covariance is approximately $(N/2)^N$ (Brigham and Morrow, 1967), where N is the linear size of the array.

If the discrete version of the Fourier transform is used to compute the cross-covariance, as in (6), the resulting function is cyclic, which is equivalent to assuming that the functions in the space domain are periodic. In other words, the Fourier transform method assumes that when movement of objects takes place, what moves out of the picture at one boundary must enter at the opposite boundary. Further examination and discussion of this assumption is presented in Section III.

The Fourier transform possesses still another property which makes it possible to take a different approach to the estimation of motion. Assume that uniform translation is the only difference between the two functions, i. e. , $g(x,y) = f(x-a, y-b)$. Then from the definition of the Fourier transform in

equation (1) it follows (Briggs, 1968) that

$$G(u,v) = F(u,v)\, e^{-2\pi i(ua+vb)} \tag{7}$$

The Fourier transform at a specific frequency (u, v) can be represented by its amplitude and phase angle in the following manner:

$$F(u,v) = |F(u,v)|\, e^{i\varphi(u,v)} \tag{8}$$

where $|F|$ is the amplitude and φ is the phase angle. Applying the same representation to G(u, v), we have

$$G(u,v) = |F(u,v)|\, e^{i\varphi(u,v)-2\pi i(ua+vb)} \tag{9}$$

Thus,

$$F^*(u,v)\, G(u,v) = |F(u,v)|^2\, e^{-2\pi i(ua+vb)} \tag{10}$$

The term $F^*(u,v)\, G(u,v)$ is complex with amplitude $|F|^2$ and phase angle $-2\pi(ua+vb)$, for all u's and v's. The differences between the phase angles of two neighboring frequencies have the following properties:

$$\varphi(u,v) - \varphi(u+1,v) = 2\pi a \tag{11}$$

and

$$\varphi(u,v) - \varphi(u,v+1) = 2\pi b \tag{12}$$

We thus find that the difference in phase angle between neighboring terms in the F*G matrix yields the x and y components of displacement.

In the case where the two images differ only in that one is a uniform translation of the other, the phase differences are the same between all neighboring frequencies. However, when the displacement between the two images is not uniform — and, specifically, when disp'acement is different for features with different characteristic dimensions — then the phase angle difference will be a function of frequency. In the following sections, we will examine to what extent the phase angle differences continue to yield estimates of the displacement and how these estimates are related to the size of features in the image.

III. SIMULATION STUDIES

A number of simulation studies were conducted to investigate the comparative effectiveness of cross-correlation and phase difference techniques for estimating motion (Lo and Parikh, 1973; Lo et al., 1974). In particular, cases were studied that involved

a. Distortions such as rotation, scale change, brightness change, and noise, in addition to simple translation

b. Mixtures of motion

c. Edge effects: objects moving off one boundary without coming back in at the opposite boundary, so that the displacements are non-cyclic.

It was found that if these conditions were not too strongly present, both techniques yielded reasonable estimates of the motion (or, in mixture cases, estimates of the predominant motion). However, as the distortion, mixture, or

edge factors become stronger, performance began to deteriorate. This situation is illustrated in the simulations shown in Figures 1 and 2.

In Figure 1, a large mass of relatively dim cloud is moving at a comparatively slow speed (displacement components $X = 2$ and $Y = 1$) relative to smaller clouds of higher brightness ($X = 4$, $Y = 6$). Figure 1a shows the two pictures, Figure 1b shows their power spectra, and Figure 1c shows their cross-covariance, which has a peak corresponding to the displacement (4, 6) of the higher-contrast clouds. Figure 1d shows the phase angles of the Fourier transform product, and Figure 1e shows the resulting X and Y displacement estimates from the phase difference method (obtained by taking horizontal and vertical differences in Figure 1d). Figure 1f is a scatter plot of these estimates, which cluster around the displacement (4, 6).

Figure 2 is analogous to Figure 1 for a pair of pictures (shown in Figure 2a) containing two sets of clouds with the same brightness but different velocities, represented by the displacements (6, 0) and (2, 2). Here the cross-covariance (Figure 2c) corresponds to the displacement (2, 2) of the larger cloud mass; but the phase difference estimates (Figure 2e) show little tendency to cluster (Figure 2f).

It would seem from these examples that the phase difference estimation approach is more sensitive to the presence of mixtures of motions than the cross-covariance approach. Similar results can be obtained by studying simulations involving edge effects and other distortions. The details can be found in the two references cited at the beginning of the section.

IV.   EXPERIMENTS WITH REAL DATA

Several experiments with pairs of real cloud windows were also carried out, as described by Lo et al. (1974). The windows used were selected from ATS-1 geosynchronous satellite images, taken at intervals of 47 minutes. Each window is 64 by 64 pixels, and has been scaled to the gray level range 0 to 63.

The two windows shown in Figure 3a contain relatively small clouds. In order to better evaluate the synoptic environment in which these cloud patterns are embedded, two larger windows (256 by 256 pixels) containing the smaller windows at their centers are shown in Figure 3b. It is evident that the clouds in this scene tend to dissipate and re-form relatively fast, so that considerable distortion has occurred between the frames. Nevertheless, many of the cloud patterns in the first window are easily recognizable in the second. Based on such patterns, a hand estimate of the relative displacement was made using computer printouts of the pictures so that the displacement could be accurately measured. The estimated displacement, averaged over several cloud elements, was $X = -5$, $Y = -3$.

The phase difference method applied to the pair of windows in Figure 3a gave rise to a displacement estimate of $(-12, -4)$. This estimate was obtained as follows: X and Y displacement estimates were obtained for each spatial frequency component. The means and standard deviations of these estimates were computed, and estimates deviating from the mean by more than

one standard deviation were discarded. The mean was then recomputed for the surviving estimates, and was used as the final estimate.

The cross-covariance method, on the other hand, yielded a displacement estimate of (-6, -3), as determined by the position of the cross-covariance peak. In this example, therefore, the cross-covariance method yields better results (assuming the hand estimate to be most reliable).

An attempt was made to improve the results obtained from the phase difference method by applying it to selected bands of spatial frequencies, rather than to all frequencies. The following results were obtained:

Band	Frequency Range	X	Y
a	$0 \leqslant \sqrt{u^2 + v^2} \leqslant 5$	-8	2
b	$5 \leqslant \sqrt{u^2 + v^2} \leqslant 10$	-13	16
c	$10 \leqslant \sqrt{u^2 + v^2} \leqslant 64$	-12	-4

Note that the last result is the same as that obtained when all frequencies were used, and that those results still do not agree very well with the hand estimate. The cross-covariance estimates were also re-evaluated using only selected spatial frequencies (i.e., the cross spectral density F*G was computed, the frequencies outside the selected band were suppressed, and the inverse Fourier transform of the result was computed to yield a "filtered" cross-covariance). The results were as follows:

Frequency Band	X	Y
a	-6	-3.5
b	-5	-3
c	No clearcut peak	

Results (a-b) are quite close to the result (-6, -3) obtained when no filtering was used, and also agree well with the hand estimate (-5, -3).

V. DISCUSSION AND CONCLUSIONS

The results of the experiments reported here indicate that both the cross-covariance and phase difference methods can be good estimators of motion when the objects being tracked do not change their shape, size and orientation to more than a limited degree. These techniques are less effective when a mixture of motions exists, unless one of the motions is strongly dominant. These properties indicate that the Fourier transform phase difference estimation methods should be reliable in problems such as landmark matching, where the features do not change appreciably as viewed in satellite photographs.

In the atmosphere, where the clouds grow, dissipate, rotate, and move relative to each other, the estimation of these motions using Fourier transform methods is not always reliable.

The main obstacle to accurate cloud motion estimation is believed to be the presence of mixtures of motions. One possible way to solve this problem is to use spatial frequency filtering to separate the motions of different types of

cloud features, since cloud size is closely related on the one hand to spatial frequency and on the other hand to cloud motion. The effort to separate clouds by their sizes through frequency filtering is, however, thwarted by the fact that for real pictures each component in the frequency domain is a complicated function of the features in the space domain. Cloud patterns are not perfect sinusoidal functions. More than one frequency component is always needed to represent a cloud element, and conversely a high frequency component may receive contributions from small cloud elements, and also from sharp corners of a large cloud element. To further complicate the matter, the small cloud element or sharp corner may not exist in the second picture with which the first picture is being correlated. It is not found possible to effectively separate cloud types by spatial frequency filtering.

Another possible approach to separating cloud types for motion estimation purposes is to segment the cloud cover windows using thresholding or pattern classification techniques (Lo and Mohr, 1974; Lo, 1975). The brightness, the equivalent black body temperature in various regions of the infrared spectrum, and the size of clouds are all closely related to the altitude of the clouds. Since clouds at certain altitudes in a limited region tend to move at the same velocity, thresholding techniques could be designed to separate clouds according to their brightness and/or spectral equivalent black body temperatures. Picture analysis techniques which determine cloud size should also be investigated for the separation of clouds.

It can be concluded from this study that a technique which separates clouds according to their motions must be designed and utilized to pre-process a picture before applying Fourier transform motion estimation techniques such as the cross-covariance and phase difference methods. The cross-covariance method appears to be somewhat more reliable than the phase difference method, and should be preferred, even though the latter does present the advantages of providing multiple estimates and relative economy in computer time.

REFERENCES

Briggs, B. H. (1968): "On the analysis of moving patterns, in Geophysics - I. Correlation analysis", J. Atmos. Terrest. Phys. 30, pp. 1777-1788.

Brigham, E. O., and R. E. Morrow (1967): "The fast Fourier transform", IEEE Spectrum, December, pp. 63-70.

Fujita, T., K. Watanabe, and T. Izawa (1969): "Formation and structure of equatorial anticyclones caused by large-scale cross-equatorial flows determined by ATS-I photographs", J. Appl. Meteor. 8, pp. 649-667.

Hubert, L. F., and L. F. Whitney, Jr. (1971): "Wind estimation from geostationary satellite pictures", Mon. Wea. Rev. 99, pp. 665-672.

Leese, J. A., and E. S. Epstein (1963): "Application of two-dimensional spectral analysis to the quantification of satellite cloud photographs," J. Appl. Meteor. 2, pp. 629-644.

Leese, J. A., C. S. Novak, and B. B. Clark (1971): "An automated technique for obtaining cloud motion from geosynchronous satellite data using cross correlation," J. App. Meteor. 10, pp. 118-132.

Lo, R. C. (1975): "The application of a thresholding technique in cloud motion estimation from satellite observations," Technical Report 357, Computer Science Center, Univ. of Maryland, College Park, Md.

Lo, R. C., and J. Mohr (1974): "Applications of enhancement and thresholding techniques to Fourier transform cloud motion estimation," Technical Report 326, Computer Science Center, Univ. of Maryland, College Park, Md.

Lo, R. C., J. Mohr, and J. A. Parikh (1974): "Applications of Fourier transform methods of cloud movement estimation to simulated and satellite photographs," Technical Report 292, Computer Science Center, Univ. of Maryland, College Park, Md.

Lo, R. C., and J. A. Parikh (1973): "A study of the application of Fourier transforms to cloud movement estimation from satellite photographs," Technical Report 242, Computer Science Center, Univ. of Maryland, College Park, Md.

Serebreny, S. M., R. G. Hadfield, R. M. Trudeau, and E. J. Wiegman (1969): "Comparison of cloud motion vectors and rawinsonde data," Final Report, Contract E-193-68 (NFSC, SSA), Stanford Research Institute, Menlo Park, CA.

Smith, E. A. and D. R. Philips (1972): "Automated cloud tracking using precisely aligned digital ATS pictures," IEEE Trans. Computers 21, pp. 715-729.

Weinstein, F. S. (1972): "An advantageous method of performing cross-correlational analysis," Proc. IEEE 60, pp. 449-450.

CAPTIONS

Figure 1

a. Gray levels of a pair of images simulating cloud motion: a large mass of
    relatively dim cloud undergoing a displacement (in pixels) of $X = 2$ and
    $Y = 1$, on which are superimposed smaller but brighter clouds under-
    going a displacement of $X = 4$, $Y = 6$.

b. Power spectra of the images in a. The $(0, 0)$ component is in the upper
    left corner, with wave number increasing downward and to the right.

c. Cross-covariance of the images in a. Zero displacement corresponds to
    the upper left corner; X displacement increases to the right and Y dis-
    placement increases downward.

d. Phase angles of the cross spectral density of the two images. The $(0,0)$
    component is in the upper left corner, with wave number increasing down-
    ward and to the right.

e. X and Y displacement estimates derived from the cross spectral density.

f. Scatter plot of the estimates in e.

Figure 2 (a-f)

Analogous to Figure 1, but for images simulating the motion of two sets of clouds
with the same brightness but different velocities (i.e., displaced by different
amounts).

Figure 3

A pair of images selected as an example from the ATS-1 satellite. (a) The
64×64 pixel portion of each image from which cloud motion is to be determined.
(b) The surrounding area (256 by 256 pixels) in which the images in a are
centrally imbedded.

GRAY LEVELS OF SECOND IMAGE

```
8  8  8  8  8  8  8  8  8  8  8  8  8  8  8  8  8  8
8  8  8  8  9  9  9  9  9  9  8  8  8  8  8  8  8  8
8  8  8  9  9  17 17 9  9  9  9  8  8  8  8  8  8  8
8  8  9  9  17 10 22 18 10 10 9  9  9  8  8  8  8  8
8  8  9  9  10 10 18 18 10 10 10 9  9  9  8  8  8  8
8  8  9  9  17 10 10 10 10 10 10 9  9  9  8  8  8  8
8  8  8  9  19 17 20 9  10 10 10 9  9  9  8  8  8  8
8  8  8  9  8  9  9  9  9  9  9  9  8  8  8  8  8  8
8  8  8  8  8  8  9  9  9  8  8  8  8  8  8  8  8  8
8  8  8  8  8  8  8  8  8  8  8  8  8  8  8  8  8  8
```

GRAY LEVELS OF FIRST IMAGE

```
8  8  8  8  8  8  8  8  8  8  8  8  8  8  8  8  8
8  8  8  8  8  9  9  9  9  9  9  8  8  8  8  8  8
8  8  8  8  9  9  9  10 10 10 10 9  8  8  8  8  8
8  8  8  9  9  10 10 10 10 10 10 9  9  8  8  8  8
8  8  8  9  9  10 10 10 10 10 9  17 10 8  8  8  8
8  8  9  9  9  10 10 10 10 10 9  17 21 17 8  8  8
8  8  9  9  9  10 10 10 10 9  9  17 17 17 8  8  8
8  8  8  8  9  8  9  9  9  9  8  8  8  8  8  8  8
8  8  8  8  8  8  18 17 8  8  8  8  8  8  8  8  8
8  8  8  8  8  8  16 18 8  8  8  8  8  8  8  8  8
8  8  8  8  8  8  8  8  8  8  8  8  8  8  8  8  8
```

Figure 1a. Gray levels of a pair of images simulating cloud motion: a large mass of relatively dim cloud undergoing a displacement (in pixels) of X = 2 and Y = 1, on which are superimposed smaller but brighter clouds undergoing a displacement of X = 4, Y = 6.

16

POWER SPECTRUM OF FIRST IMAGE

8.73	0.51	0.15	0.13	0.19	0.13	0.05	0.03	0.01	0.03	0.05	0.13	0.19	0.13	0.15	0.51
0.47	0.28	0.10	0.08	0.18	0.12	0.06	0.04	0.05	0.04	0.06	0.12	0.19	0.16	0.09	0.39
0.28	0.29	0.16	0.05	0.14	0.12	0.03	0.06	0.06	0.06	0.03	0.12	0.17	0.18	0.07	0.16
0.26	0.26	0.15	0.02	0.12	0.10	0.01	0.07	0.07	0.07	0.01	0.10	0.15	0.15	0.08	0.13
0.18	0.22	0.15	0.01	0.09	0.08	0.03	0.04	0.06	0.04	0.03	0.10	0.11	0.14	0.10	0.06
0.10	0.16	0.14	0.05	0.05	0.07	0.03	0.05	0.06	0.05	0.03	0.06	0.07	0.09	0.08	0.01
0.05	0.10	0.10	0.05	0.06	0.05	0.01	0.03	0.05	0.03	0.01	0.04	0.03	0.05	0.07	0.03
0.00	0.04	0.06	0.06	0.04	0.02	0.01	0.02	0.04	0.02	0.01	0.03	0.02	0.02	0.04	0.03
0.02	0.01	0.01	0.02	0.02	0.01	0.00	0.01	0.02	0.01	0.00	0.01	0.02	0.02	0.01	0.01
0.00	0.03	0.04	0.02	0.02	0.03	0.02	0.03	0.04	0.03	0.02	0.03	0.04	0.06	0.06	0.04
0.05	0.03	0.07	0.05	0.03	0.04	0.03	0.03	0.05	0.03	0.03	0.05	0.06	0.05	0.10	0.10
0.10	0.01	0.08	0.09	0.07	0.06	0.04	0.03	0.06	0.05	0.05	0.07	0.09	0.01	0.14	0.16
0.18	0.06	0.10	0.14	0.11	0.10	0.07	0.05	0.07	0.05	0.06	0.08	0.12	0.02	0.15	0.22
0.26	0.13	0.08	0.15	0.15	0.11	0.06	0.05	0.06	0.03	0.05	0.10	0.14	0.05	0.16	0.26
0.28	0.16	2.07	0.18	0.17	0.11	0.05	0.03	0.05	0.04	0.06	0.12	0.18	0.05	0.16	0.29
0.47	0.38	0.09	0.16	0.19	0.13	0.05	0.04	0.05	0.02	0.04	0.12	0.18	0.08	0.10	0.28

POWER SPECTRUM OF SECOND IMAGE

8.73	0.54	0.16	0.15	0.19	0.13	0.07	0.03	0.01	0.03	0.07	0.13	0.19	0.15	0.16	0.54
0.56	0.42	0.14	0.11	0.17	0.13	0.05	0.04	0.02	0.04	0.05	0.13	0.19	0.16	0.10	0.40
0.33	0.29	0.15	0.05	0.15	0.13	0.03	0.05	0.04	0.05	0.03	0.11	0.17	0.16	0.03	0.21
0.25	0.27	0.16	0.02	0.13	0.12	0.03	0.05	0.07	0.05	0.03	0.08	0.15	0.16	0.06	0.13
0.17	0.21	0.14	0.02	0.08	0.08	0.03	0.04	0.08	0.04	0.04	0.07	0.11	0.14	0.10	0.05
0.12	0.17	0.13	0.05	0.05	0.07	0.03	0.04	0.08	0.04	0.06	0.06	0.07	0.09	0.07	0.01
0.06	0.10	0.10	0.05	0.02	0.06	0.02	0.04	0.06	0.04	0.08	0.02	0.03	0.06	0.05	0.01
0.01	0.02	0.04	0.03	0.01	0.03	0.01	0.02	0.04	0.02	0.08	0.02	0.01	0.03	0.04	0.03
0.02	0.01	0.02	0.02	0.01	0.02	0.01	0.03	0.05	0.03	0.05	0.03	0.02	0.03	0.02	0.01
0.01	0.03	0.04	0.03	0.02	0.04	0.02	0.04	0.04	0.04	0.04	0.05	0.03	0.05	0.04	0.02
0.06	0.01	0.05	0.06	0.04	0.04	0.03	0.06	0.06	0.06	0.06	0.07	0.05	0.05	0.10	0.10
0.12	0.01	0.07	0.09	0.05	0.06	0.05	0.08	0.06	0.08	0.08	0.07	0.08	0.02	0.13	0.17
0.17	0.05	0.10	0.11	0.07	0.07	0.07	0.08	0.04	0.08	0.08	0.12	0.13	0.02	0.14	0.21
0.25	0.13	0.06	0.15	0.08	0.08	0.08	0.06	0.05	0.06	0.07	0.12	0.15	0.05	0.16	0.27
0.33	0.21	0.03	0.16	0.11	0.11	0.06	0.05	0.05	0.04	0.04	0.13	0.17	0.05	0.15	0.29
0.56	0.40	0.10	0.16	0.13	0.13	0.07	0.02	0.02	0.04	0.02	0.13	0.17	0.11	0.14	0.42

Figure 1b. Power spectra of the images in a. The (0,0) component is in the upper left corner, with wave number increasing downward and to the right.

CROSS-COVARIANCE FUNCTION

76.4	76.7	76.7	76.6	76.4	76.2	76.0	75.8	75.7	75.6	75.7	75.7	75.9	76.0	76.2
76.6	77.0	77.0	76.9	76.6	76.4	76.1	75.9	75.8	75.7	75.7	75.8	75.9	76.0	76.3
76.7	77.1	77.2	77.1	76.8	76.6	76.3	76.0	75.9	75.7	75.7	75.8	75.9	76.1	76.4
76.8	77.2	77.3	77.2	77.0	76.6	76.4	76.1	75.9	75.6	75.6	75.8	75.9	76.2	76.5
76.7	77.2	77.5	77.4	77.1	76.8	76.9	76.6	76.1	75.6	75.7	75.7	75.9	76.1	76.5
76.8	77.2	78.1	78.7	77.9	77.2	77.4	77.2	76.3	75.7	75.8	75.7	75.9	76.0	76.3
77.3	77.5	78.6	79.9	78.4	77.1	77.0	76.8	76.0	75.7	75.7	75.7	75.8	75.9	76.3
77.4	77.2	77.6	78.2	77.4	76.3	76.2	76.0	75.7	75.7	75.7	75.6	75.7	75.8	76.5
76.4	76.3	76.3	76.3	76.2	75.9	75.8	75.7	75.7	75.6	75.6	75.6	75.6	75.7	76.1
75.7	75.9	75.9	75.8	75.8	75.7	75.7	75.7	75.6	75.6	75.6	75.6	75.6	75.6	75.7
75.7	75.8	75.8	75.7	75.7	75.6	75.6	75.6	75.6	75.6	75.6	75.6	75.6	75.6	75.7
75.7	75.7	75.7	75.7	75.7	75.7	75.6	75.6	75.6	75.6	75.6	75.6	75.7	75.7	75.7
75.8	75.8	75.8	75.8	75.7	75.7	75.7	75.7	75.6	75.6	75.6	75.6	75.7	75.7	75.7
75.8	75.9	76.0	75.9	75.8	75.7	75.7	75.7	75.6	75.6	75.6	75.7	75.7	75.7	75.8
76.0	76.1	76.1	76.1	76.1	75.8	75.9	75.7	75.6	75.6	75.6	75.7	75.8	75.8	75.9
76.2	76.4	76.4	76.3	76.2	76.0	75.7	75.7	75.7	75.6	75.7	75.7	75.8	75.9	76.1

Figure 1c. Cross-covariance of the images in a. Zero displacement corresponds to the upper left corner; X displacement increases to the right and Y displacement increases downward.

PHASE ANGLES OF CROSS SPECTRAL DENSITY

0.0	-3.1	-6.2	4.3	0.0	-3.7	7.0	4.2	0.0	-4.2	-7.0	3.7	0.0	-4.3	6.2	3.1
-4.1	7.9	2.5	-1.8	-5.9	6.1	2.3	-2.0	-4.9	7.2	3.2	-2.0	-5.9	6.0	2.3	-0.8
-4.5	0.2	-4.2	8.0	3.9	-0.1	-2.5	7.4	4.1	1.0	-3.5	8.0	3.9	0.2	-5.2	-7.7
-2.0	-6.0	6.1	-3.5	-2.3	-5.6	6.6	1.8	-2.0	-6.0	5.2	1.6	-2.0	-6.0	5.9	1.7
7.8	3.8	0.1	-4.8	-7.6	4.3	0.0	-4.6	8.0	4.8	-0.6	-4.8	8.0	3.8	0.0	-4.1
1.5	-2.4	-6.3	5.7	1.7	-1.9	-3.9	5.5	2.3	-1.1	-5.3	5.9	2.0	-2.1	-5.9	0.0
-4.5	8.0	4.2	-0.2	-3.0	-6.5	5.8	0.1	-4.0	8.0	3.1	-0.7	-3.1	7.8	4.2	1.3
-7.7	1.5	-1.9	-4.9	-6.4	3.5	-2.5	-6.1	6.0	2.1	-3.1	7.5	2.0	0.7	-2.1	-6.0
0.0	-4.5	7.3	4.2	0.0	-4.4	2.7	2.9	0.0	-2.9	-2.7	4.4	0.0	-4.2	-7.3	4.5
7.7	6.0	2.1	-0.7	-2.0	-7.5	3.1	-2.1	-6.0	6.1	2.5	-3.5	6.4	4.9	1.9	-1.5
4.5	-1.3	-4.2	-7.8	3.1	0.7	-3.1	8.0	4.0	-0.1	-5.8	6.5	3.0	0.2	-4.2	8.0
-1.5	0.0	5.9	2.1	-2.0	-5.9	5.3	1.1	-2.3	-5.5	3.9	1.9	-1.7	-5.7	6.3	2.4
-7.8	4.1	0.0	-3.8	-8.0	4.8	0.6	-4.8	-8.0	4.6	0.0	-4.3	7.6	4.8	-0.1	-3.8
2.0	-1.7	-5.9	6.0	2.0	-1.6	-5.2	6.0	2.0	-1.8	-6.6	5.6	2.3	3.5	-6.1	6.0
-4.5	7.7	5.2	-0.2	-3.9	8.0	3.5	-1.0	-4.1	-7.4	2.5	0.1	-3.9	8.0	4.2	-0.2
4.1	0.8	-2.3	-6.0	5.9	2.0	-3.2	-7.2	4.9	2.0	-2.3	-6.1	5.9	1.8	-2.5	-7.9

Figure 1d. Phase angles of the cross spectral density of the two images. The (0,0) component is in the upper left corner, with wave number increasing downward and to the right.

X DISPLACEMENT ESTIMATES

3.1	3.2	5.4	4.3	3.7	5.2	2.8	4.2	4.2	2.8	5.2	3.7	4.3	5.4	3.2	3.1
4.0	5.4	4.4	4.1	4.0	3.7	4.3	2.9	3.9	4.0	5.3	3.9	4.1	3.6	3.1	3.3
4.3	4.4	3.8	4.1	3.9	2.5	6.1	3.3	3.1	4.5	3.6	4.1	3.8	5.4	2.5	3.8
4.0	3.9	-6.4	-1.1	3.2	3.8	4.8	3.4	3.9	4.8	3.6	3.6	4.0	4.1	4.2	3.7
4.0	3.7	4.9	2.7	4.1	4.3	4.6	3.4	3.2	5.4	4.2	3.2	4.2	3.8	4.1	4.2
3.9	4.0	3.9	4.0	3.7	-1.9	6.6	3.2	3.4	4.3	4.7	3.9	4.1	3.8	-5.9	-1.6
3.5	3.8	4.3	2.8	3.5	3.7	5.7	4.0	4.0	4.9	3.9	2.3	5.1	3.6	3.0	5.7
6.8	3.5	3.0	1.5	6.1	6.0	3.6	3.9	3.9	5.2	5.4	5.5	1.3	2.9	3.2	1.7
4.5	4.2	3.0	4.2	4.4	-7.1	-0.3	2.9	2.9	-0.3	-7.1	4.4	4.2	3.0	4.2	4.5
1.7	3.9	2.9	-1.3	5.5	5.4	5.2	3.9	3.9	3.6	6.0	5.5	1.5	3.0	3.5	6.8
5.7	3.0	3.6	5.1	2.3	3.9	4.9	4.0	4.0	5.7	3.7	2.3	2.8	4.3	3.8	3.5
-1.6	-5.9	3.8	4.1	3.9	4.7	4.3	3.4	3.2	6.6	1.9	3.9	4.0	3.9	4.0	3.9
4.2	4.1	3.8	4.2	3.2	4.2	5.7	3.2	3.9	4.6	4.3	3.2	2.7	4.9	3.7	4.0
3.7	4.2	4.1	4.0	3.6	3.6	4.8	3.9	3.1	4.8	3.8	3.6	-1.1	-6.4	3.9	4.5
3.8	2.5	5.4	3.8	4.1	4.5	4.5	3.3	3.9	6.1	2.5	4.1	4.1	3.8	4.4	4.3
3.3	3.1	3.6	4.1	3.9	5.3	4.0	2.9	3.9	4.7	3.7	3.9	4.1	4.4	5.4	4.0

Y DISPLACEMENT ESTIMATES

4.1	5.0	7.2	6.2	5.9	6.2	4.7	6.2	4.9	4.5	5.8	5.9	5.7	3.9	3.9
7.4	7.7	6.7	6.2	6.2	6.1	4.8	6.6	7.0	6.2	6.7	6.2	5.8	7.5	6.9
6.5	6.2	5.7	-4.5	6.2	5.5	6.9	5.5	6.1	6.9	7.3	5.9	6.2	4.9	6.6
6.2	6.2	6.0	1.4	5.2	6.1	6.6	6.4	6.0	5.2	5.8	6.0	6.1	5.9	5.8
6.2	6.1	6.4	5.4	6.7	6.3	3.9	5.9	5.7	5.9	4.7	6.0	5.9	5.9	-4.0
6.0	5.6	5.5	5.9	4.7	4.6	6.3	5.5	6.3	6.9	7.5	5.1	6.1	5.9	-1.3
3.2	6.5	6.1	4.7	3.4	6.0	-7.7	6.1	6.0	5.9	6.2	-5.1	7.1	6.3	7.2
-7.7	6.1	6.8	6.9	-6.4	7.9	-5.2	7.0	6.0	5.1	-0.4	2.0	5.0	5.2	5.5
-7.7	5.5	5.2	5.0	2.0	3.1	-0.4	5.1	6.0	7.0	-5.2	-6.4	6.9	6.8	6.1
3.2	7.2	6.3	7.1	-5.1	7.8	6.2	5.9	6.3	6.1	-7.7	3.4	4.7	6.1	6.5
6.0	-1.3	5.9	6.1	5.1	6.6	7.5	5.2	5.7	5.5	3.9	4.7	5.9	5.5	5.6
6.2	-4.0	5.9	5.9	6.0	5.3	4.7	6.9	6.0	5.9	6.6	6.7	5.4	6.4	6.1
6.2	5.8	5.9	6.1	6.0	6.4	5.8	5.2	6.1	6.4	6.9	5.2	1.4	6.0	6.2
6.5	6.6	4.9	6.2	5.9	6.0	7.3	6.9	7.0	5.5	4.8	6.2	-4.5	5.7	6.2
7.4	6.9	7.5	5.8	6.2	6.0	6.7	6.2	6.1	6.6	4.7	6.2	6.2	6.7	7.7
4.1	3.9	3.9	5.7	5.9	5.8	5.8	4.5	4.9	6.2	5.9	6.2	6.2	7.2	5.0

Figure 1e.   X and Y displacement estimates derived from the cross spectral density.
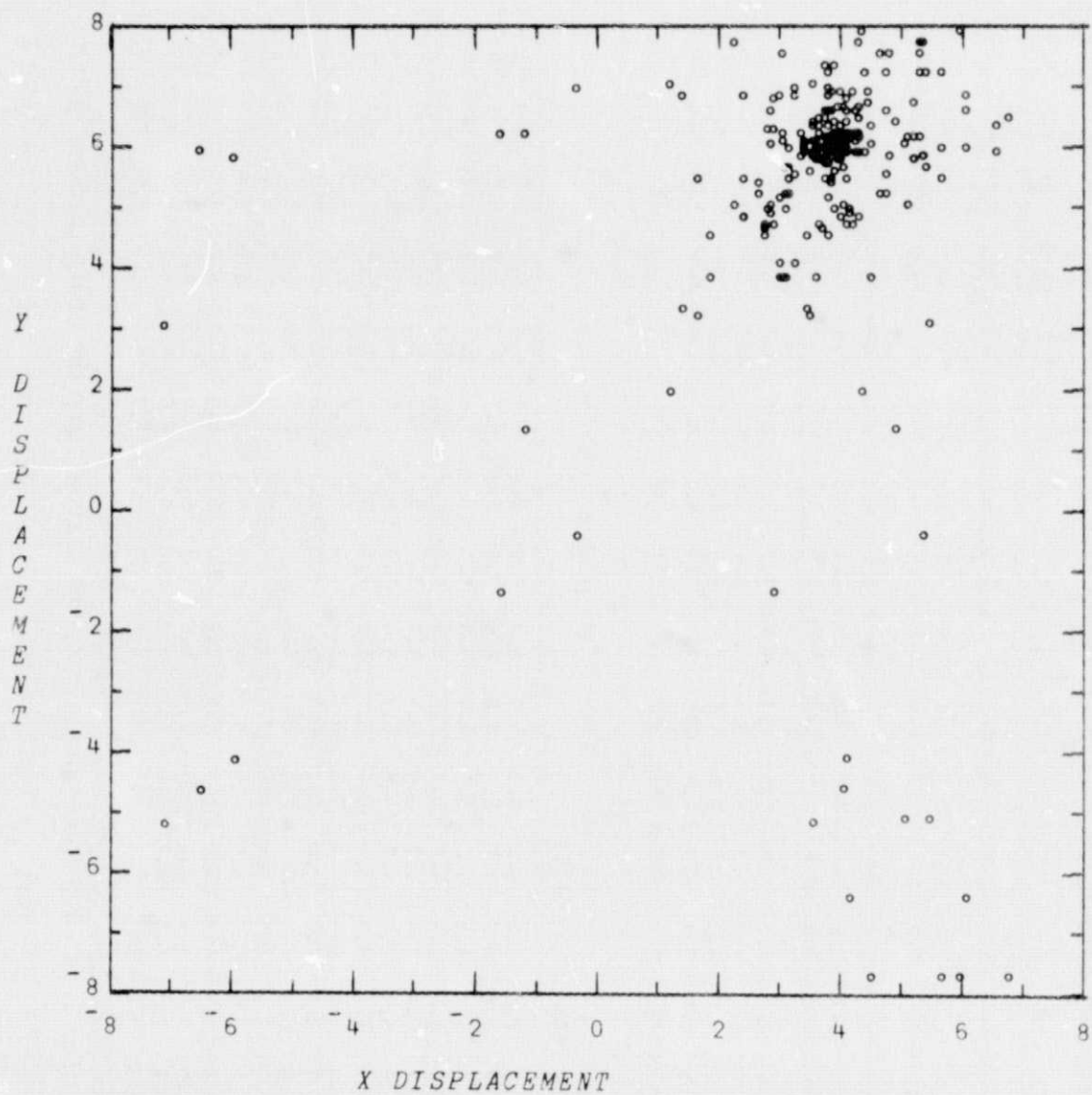
Figure 1f. Scatter plot of the estimates in e.

GRAY LEVELS OF SECOND IMAGE

GRAY LEVELS OF FIRST IMAGE

Figure 2a. Analogous to Figure 1, but for images simulating the motion of two sets of clouds with the same brightness but different velocities (i.e., displaced by different amounts).

21

POWER SPECTRUM OF FIRST IMAGE

5.86	3.81	0.33	1.23	0.52	0.26	0.38	0.22	0.08	0.22	0.38	0.26	0.52	1.23	0.33	3.81
1.28	1.26	0.76	0.64	0.27	0.15	0.16	0.06	0.12	0.08	0.13	0.14	0.10	0.32	0.82	1.01
2.06	0.94	0.62	0.71	0.09	0.11	0.14	0.22	0.30	0.33	0.22	0.07	0.12	0.91	0.72	1.00
1.12	0.71	0.51	0.11	0.38	0.16	0.36	0.27	0.02	0.11	0.24	0.26	0.13	0.06	0.38	0.81
0.52	0.34	0.07	0.25	0.28	0.19	0.28	0.36	0.39	0.04	0.42	0.06	0.67	0.46	0.09	0.28
0.36	0.19	0.14	0.54	0.45	0.32	0.53	0.07	0.39	0.12	0.22	0.20	0.33	0.38	0.11	0.17
0.26	0.14	0.14	0.40	0.34	0.26	0.41	0.31	0.14	0.19	0.38	0.32	0.29	0.35	0.12	0.14
0.30	0.01	0.22	0.14	0.32	0.10	0.20	0.44	0.05	0.47	0.27	0.10	0.27	0.19	0.23	0.02
0.08	0.17	0.32	0.19	0.32	0.39	0.32	0.55	0.08	0.55	0.32	0.39	0.32	0.19	0.32	0.17
0.30	0.02	0.23	0.19	0.27	0.10	0.27	0.47	0.05	0.44	0.20	0.10	0.32	0.14	0.22	0.01
0.26	0.14	0.12	0.35	0.28	0.32	0.38	0.19	0.14	0.31	0.41	0.26	0.34	0.40	0.14	0.14
0.36	0.17	0.11	0.38	0.33	0.20	0.22	0.12	0.39	0.07	0.53	0.32	0.45	0.54	0.14	0.19
0.52	0.28	0.09	0.46	0.67	0.36	0.42	0.04	0.39	0.36	0.28	0.19	0.28	0.25	0.07	0.34
1.12	0.81	0.38	0.06	0.13	0.26	0.24	0.11	0.02	0.27	0.36	0.15	0.38	0.11	0.51	0.71
2.06	1.00	0.72	0.91	0.12	0.07	0.22	0.33	0.30	0.22	0.14	0.11	0.09	0.71	0.62	0.94
1.28	1.01	0.82	0.32	0.10	0.14	0.13	0.08	0.12	0.06	0.16	0.15	0.27	0.64	0.76	1.26

POWER SPECTRUM OF SECOND IMAGE

5.86	2.78	1.30	1.15	0.52	0.20	0.30	0.28	0.06	0.28	0.30	0.20	0.52	1.15	1.30	2.78
1.28	1.98	0.17	0.82	0.10	0.16	0.18	0.08	0.12	0.09	0.16	0.17	0.27	0.46	0.35	2.58
2.06	0.94	0.15	0.58	0.12	0.11	0.08	0.31	0.30	0.33	0.19	0.13	0.09	0.91	0.41	0.49
1.12	0.87	0.61	0.12	0.13	0.22	0.38	0.20	0.02	0.16	0.27	0.13	0.38	0.05	0.51	0.10
0.52	0.06	0.07	0.15	0.67	0.09	0.28	0.28	0.39	0.23	0.42	0.18	0.28	0.50	0.09	0.43
0.36	0.10	0.11	0.56	0.33	0.17	0.49	0.09	0.39	0.10	0.09	0.26	0.45	0.31	0.07	0.20
0.26	0.17	0.08	0.40	0.28	0.35	0.40	0.31	0.14	0.29	0.37	0.32	0.34	0.32	0.03	0.14
0.30	0.06	0.28	0.16	0.27	0.11	0.27	0.42	0.05	0.43	0.32	0.10	0.32	0.23	0.29	0.04
0.08	0.12	0.28	0.19	0.32	0.40	0.42	0.50	0.08	0.50	0.42	0.49	0.32	0.19	0.28	0.12
0.30	0.04	0.27	0.23	0.32	0.10	0.32	0.43	0.05	0.42	0.27	0.11	0.27	0.16	0.28	0.06
0.26	0.14	0.03	0.32	0.34	0.32	0.37	0.29	0.14	0.31	0.40	0.35	0.28	0.40	0.03	0.17
0.36	0.20	0.07	0.31	0.45	0.26	0.09	0.10	0.39	0.09	0.49	0.17	0.33	0.56	0.11	0.10
0.52	0.43	0.09	0.50	0.28	0.18	0.42	0.23	0.02	0.28	0.28	0.09	0.67	0.15	0.07	0.06
1.12	0.10	0.51	0.05	0.38	0.13	0.27	0.16	0.30	0.20	0.38	0.22	0.13	0.12	0.61	0.87
2.06	0.49	0.41	0.91	0.09	0.13	0.19	0.33	0.31	0.30	0.18	0.11	0.12	0.58	0.15	0.94
1.28	2.58	0.35	0.46	0.27	0.17	0.16	0.09	0.12	0.08	0.18	0.16	0.10	0.82	0.17	1.98

Figure 2b. Power spectra of the images in a. The (0,0) component is in the upper left corner, with wave number increasing downward and to the right.

22

CROSS-COVARIANCE FUNCTION

54.7	70.3	67.2	64.1	60.9	60.9	64.1	42.2	26.6	17.2	15.6	23.4	20.3	25.0	29.7	43.8
62.5	71.9	75.0	71.9	65.6	62.5	53.1	43.8	25.0	15.6	12.5	15.6	21.9	25.0	34.4	43.8
57.8	70.3	82.8	67.2	60.9	53.1	45.3	31.3	20.3	7.8	9.4	10.9	17.2	23.4	29.7	45.3
53.1	62.5	65.6	59.4	53.1	43.8	34.4	25.0	9.4	4.7	3.1	6.3	12.5	18.8	28.1	39.1
45.3	53.1	54.7	56.3	48.4	40.6	29.7	17.2	10.9	6.3	3.1	6.3	7.8	17.2	26.6	37.5
42.2	50.0	56.3	53.1	50.0	43.8	34.4	25.0	14.1	7.8	7.8	6.3	12.5	18.8	26.6	35.9
43.8	54.7	59.4	59.4	54.7	50.0	43.8	32.8	21.9	15.6	14.1	14.1	17.2	20.3	28.1	34.4
46.9	56.3	60.9	62.5	59.4	56.3	48.4	40.6	31.3	23.4	20.3	21.9	21.9	25.0	26.6	35.9
43.8	56.3	62.5	57.8	54.7	54.7	53.1	46.9	35.9	26.6	23.4	26.6	28.1	26.6	25.0	32.8
39.1	54.7	59.4	53.1	50.0	50.0	56.3	51.6	35.9	28.1	26.6	28.1	31.3	28.1	26.6	28.1
35.9	46.9	54.7	48.4	46.9	48.4	51.6	46.9	35.9	26.6	23.4	26.6	28.1	26.6	23.4	26.6
34.4	40.6	45.3	46.9	46.9	43.8	42.2	37.5	31.3	23.4	20.3	21.9	21.9	21.9	20.3	23.4
28.1	37.5	40.6	40.6	39.1	37.5	34.4	26.6	20.3	15.5	14.1	15.6	15.6	14.1	15.6	21.9
26.6	34.4	37.5	34.4	31.3	34.4	28.1	21.9	7.8	7.8	10.9	9.4	9.4	9.4	14.1	20.3
32.8	37.5	39.1	39.1	39.1	37.5	32.8	20.3	14.1	7.8	9.4	9.4	7.8	12.5	17.2	26.6
46.9	50.0	53.1	50.0	53.1	53.1	43.8	37.5	21.9	14.1	12.5	12.5	18.8	18.8	25.0	35.9

Figure 2c. Cross-covariance of the images in a. Zero displacement corresponds to the upper left corner; X displacement increases to the right and Y displacement increases downward.

PHASE ANGLES OF CROSS SPECTRAL DENSITY

0.0	-2.8	-6.2	-3.1	8.0	6.0	5.6	3.6	0.0	-3.6	-5.6	-6.0	8.0	3.1	6.2	2.8
-5.0	-3.9	3.2	1.2	7.2	3.9	1.1	3.9	-2.0	-5.3	-5.0	-7.8	7.2	-0.3	-2.2	-1.3
-1.4	-6.0	6.6	-6.2	5.3	2.0	-6.4	-0.6	-4.0	-6.0	5.3	6.3	5.3	2.0	-1.8	4.6
-1.6	-7.1	5.6	2.2	-0.7	0.1	-3.7	7.6	-6.0	-5.2	3.5	3.3	-0.7	-1.5	-2.0	-0.1
2.4	6.3	4.0	7.5	3.4	-0.1	-4.0	7.9	8.0	-1.1	4.0	0.2	3.4	-0.1	-4.0	-7.7
3.2	3.0	2.5	-1.3	-7.0	-3.4	-5.2	-7.5	6.0	5.0	0.0	-0.1	-7.0	4.7	-5.9	7.6
5.7	2.4	1.6	-2.0	-7.3	-6.2	-7.8	6.0	4.0	-4.4	-0.2	-2.0	-7.3	3.0	-7.3	6.0
1.1	6.3	-2.2	-0.9	-7.0	7.9	-2.4	6.2	2.0	-6.4	2.7	-4.0	-7.0	0.1	6.3	5.3
0.0	-2.9	-3.8	-2.3	8.0	6.0	-2.1	6.3	0.0	-6.3	2.1	-6.0	8.0	2.3	3.8	2.9
-1.1	-5.3	-6.3	-0.1	7.0	4.0	-2.7	6.4	-2.0	-6.2	2.4	-7.9	7.0	0.9	2.2	-6.3
-5.7	-6.0	7.3	-3.0	7.3	2.0	0.2	4.4	-4.0	-6.0	7.8	6.2	7.3	2.0	-1.6	-2.4
-3.2	-7.6	5.9	-4.7	7.0	0.1	0.0	-5.0	-6.0	7.5	5.2	3.4	7.0	1.3	-2.5	-3.0
-2.4	7.7	4.0	0.1	-3.4	-0.2	-4.0	1.1	8.0	-7.9	4.0	0.1	-3.4	-7.5	-4.0	-6.3
1.6	0.1	2.0	1.5	0.7	-3.3	-3.5	5.2	6.0	-7.6	3.7	-0.1	0.7	-2.2	-5.6	7.1
1.4	-4.6	1.8	-2.0	-5.3	-6.3	-5.3	6.0	4.0	0.6	6.4	-2.0	-5.3	6.2	-6.6	6.0
5.0	1.3	2.2	0.3	-7.2	7.8	5.0	5.3	2.0	-3.9	-1.1	-3.9	-7.2	-1.2	-3.2	3.9

Figure 2d. Phase angles of the cross spectral density of the two images. The (0,0) component is in the upper left corner, with wave number increasing downward and to the right.

24

X DISPLACEMENT ESTIMATES

```
 2.8  3.3 -3.0  4.9  2.0  0.5  2.0  3.6  3.6  2.0  0.5  2.0  4.9 -3.0  3.3  2.8
-1.2 -7.1  2.0 -6.0  3.3  2.8 -2.8  5.9  3.3 -0.3  2.9  0.9  7.6  1.9 -1.0  3.8
 4.6  3.4 -3.2  4.4  3.3 -7.6 -5.8  3.4  2.0  4.7 -0.9  0.9  3.3  3.8 -6.4  5.9
 5.5  3.3  3.4  2.8 -0.8  3.8  4.7 -2.4 -0.8  7.3  0.2  4.0  0.9  0.4 -1.8  1.5
-3.9  2.3 -3.5  4.1  3.6  3.9  4.1 -0.1 -6.9 -5.1  3.8 -3.2  3.5  3.6  3.7  5.9
 0.2  0.5  3.9  5.7 -3.6  1.8  2.4  2.5  1.0  5.0  0.1  6.9  4.3  3.9  2.5  4.3
 3.3  0.8  3.6  5.3 -1.1  1.6  2.2  2.0 -7.6 -4.2  1.8  5.3  5.7  5.7  2.7  0.3
-5.2 -7.4 -1.3  6.0  1.1 -5.7  7.5  4.2 -7.6  7.0  6.6  7.0 -7.0 -6.2 -1.6  4.2
 2.9  0.9 -1.6  5.7  2.0 -7.9  7.6  6.3  6.3  7.6 -7.9  2.0  5.7 -1.6  0.9  2.9
 4.2  1.0 -6.2 -7.0  3.0  6.6  7.0 -7.6  4.2  7.5 -5.7  1.1  6.0 -1.3 -7.4 -5.2
 0.3  2.7 -5.7  5.7  5.3  1.8 -4.2 -7.6  2.0  2.2  1.6 -1.1  5.3  3.6  0.8  3.3
 4.3  2.5 -5.5  4.3  6.9  0.1  5.0  1.0  2.5  2.4  1.8 -3.6  5.7 -3.5  0.5  0.2
 5.9  3.7  3.9  3.5 -3.2  3.8 -5.1 -6.9 -0.1  4.1  3.9  3.6  4.1  3.4  3.3 -3.9
 1.5 -1.8  0.4  0.9  4.0  0.2  7.3 -0.8 -2.4  4.7  3.8 -0.8  2.8  3.3  3.3  5.5
 5.9 -6.4  3.8  3.3  0.9 -0.9  4.7  2.0  3.4 -5.8 -7.6  3.3  4.4 -3.2  3.4  4.6
 3.8 -1.0  1.9  7.6  0.9  2.9 -0.3  3.3  5.9 -2.8  2.8  3.3 -6.0  2.0 -7.1  2.8
```

Y DISPLACEMENT ESTIMATES

```
 5.0  1.0  6.6 -4.4  0.8  2.1  4.5 -0.4  2.0  1.7 -0.6  1.8  0.8  3.5  4.1
-3.7  2.1 -3.4  7.5  1.9  1.9  7.5  4.6  2.0  0.7  5.7  1.9  1.9 -2.3 -5.8
 0.2  1.1  1.0  7.6  6.0  1.9 -2.8  7.8  2.0 -0.8  1.8  2.9  6.0  3.5  4.7
-4.0  2.7  1.6 -5.3 -4.1  0.3  0.3 -0.3  2.0 -4.1 -0.5  3.1 -4.1 -1.4  7.6
-0.9  3.2  1.5 -7.2 -5.6  3.3  1.2 -0.5  2.0 -6.1  0.2  0.4 -5.6 -4.7  0.7
-2.4  0.7  1.0  0.7  0.3  2.7  2.6  2.5  2.0 -6.7 -2.9  1.9  0.3  1.6 -1.6
 4.6 -3.9  3.8 -1.1 -0.3  1.9 -5.4 -0.2  2.0  2.0  0.6  2.0 -0.3  3.0  0.7
 1.1 -6.8  1.6  1.4 -0.3  2.0 -0.3 -0.1  2.0 -0.1  0.6  2.0  1.0 -2.2  2.3
 1.1  2.3  2.5 -2.2  1.0  2.0  0.6 -0.1  2.0 -0.1 -0.3  2.0  1.0  1.4 -6.8
 4.6  0.7  2.4  3.0 -0.3  2.0 -2.9  2.0  2.0 -0.2 -5.4  1.9 -0.3 -1.1 -3.9
-2.4  1.6  1.4  1.6  0.3  1.9  0.2 -6.7  2.0  2.5  2.6  2.7  0.7 -7.2  0.7
-0.9  0.7  1.9 -4.7 -5.6  0.4  4.0 -6.1  2.0 -0.5  1.2  3.3 -5.6  1.5  3.2
-4.0  7.6  2.0 -1.4 -4.1  3.1 -0.5 -4.1  2.0 -0.3 -2.8  0.3 -4.1  1.6  2.7
-0.2  4.7  0.1  3.5  6.0  2.9  1.8 -0.8  2.0  7.8  7.5  1.9  6.0  7.5  1.1
-3.7 -5.8 -0.4 -2.3  1.9  1.9  5.7  0.7  2.0  4.6  1.9  0.8  1.9  7.5  2.1
 5.0  4.1 -7.6  3.5  0.8  1.8 -0.6  1.7  2.0 -0.4  4.5 -0.6  0.8 -4.4  1.0
```

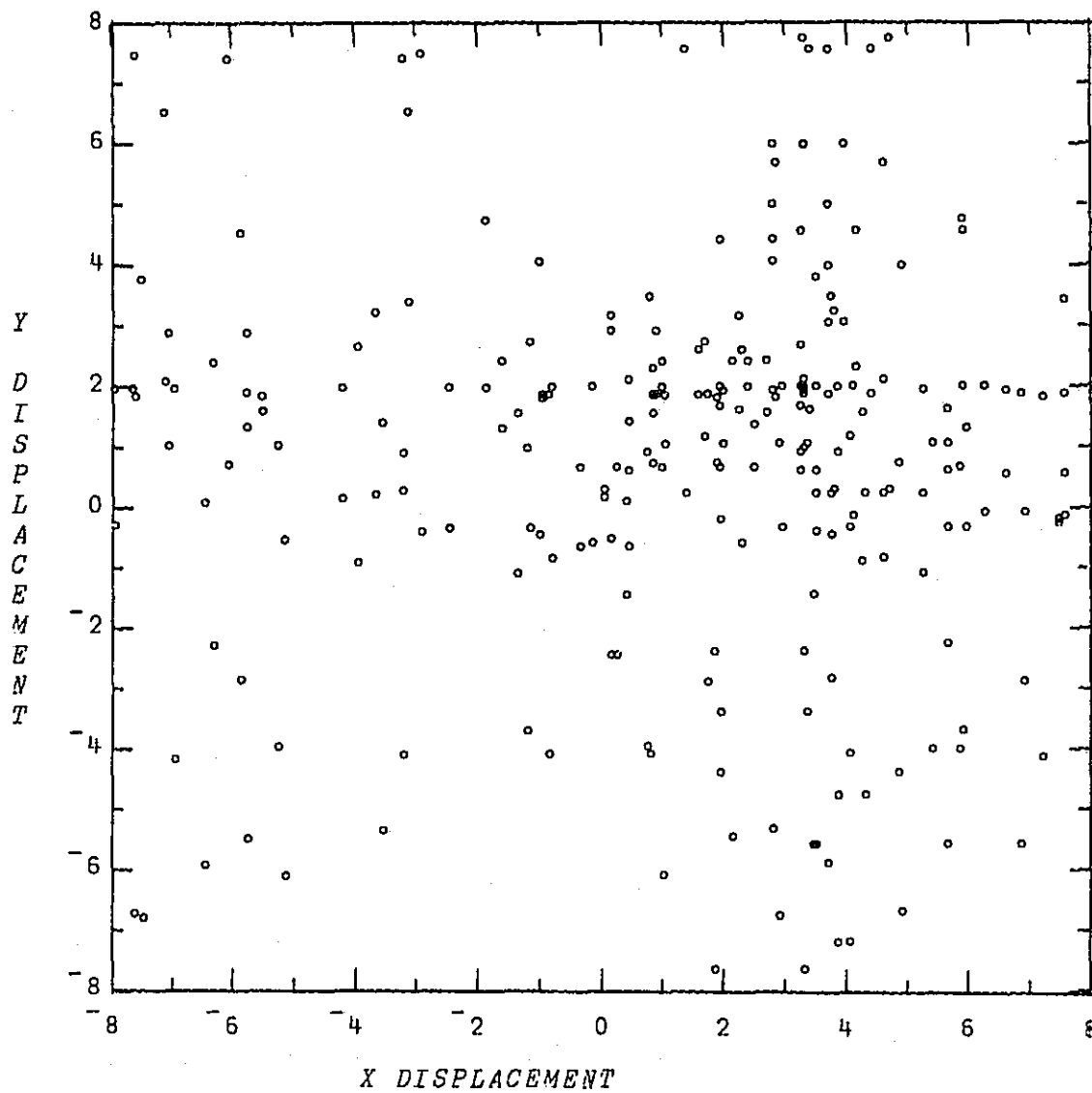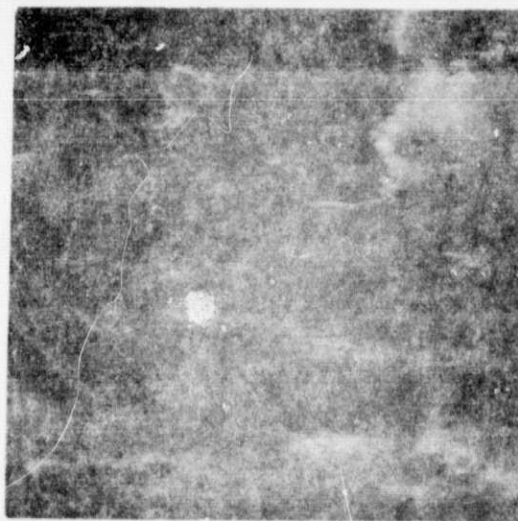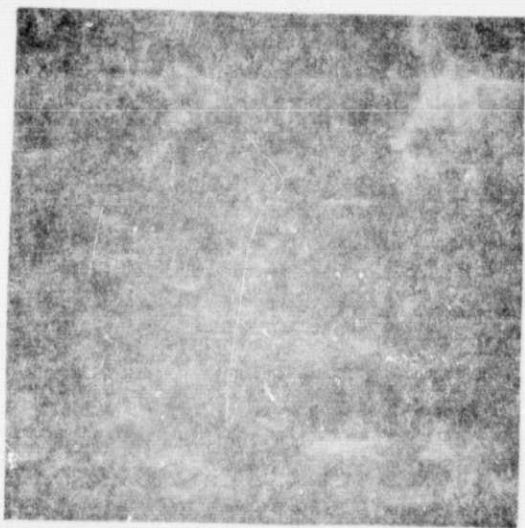Figure 2e. X and Y displacement estimates derived from the cross spectral density.

Figure 2f. Scatter plot of the estimates in e.

3a

3b

Figure 3. A pair of images selected as an example from the ATS-1 satellite. (a) The 64×64 pixel portion of each image from which cloud motion is to be determined. (b) The surrounding area (256 by 256 pixels) in which the images in a are centrally imbedded.